Journal of
Polymer Materials

Tech Science Press

https://doi.org/10.32604/jpm.2026.073634

ARTICLE

Biocomposite Films Integrating/Combining Collagen and *Lonchocarpus cyanescens* Fiber-Derived Carboxymethylcellulose for Food Packaging: Synthesis, Preparation and Characterization

Edja Florentin Assanvo[1,*], N'Dri N'Guessan Gervais Ziabo[1], Kohi Alfred Kouame[2] and David Boa[1]

[1]Laboratoire de Thermodynamique et de Physico-Chimie du Milieu, UFR des Sciences Fondamentales et Appliquées, Université Nangui ABROGOUA, Abidjan, Côte d'Ivoire
[2]UFR des Sciences et Technologie des Aliments, Université Nangui ABROGOUA, Abidjan, Côte d'Ivoire

*Corresponding Author: Edja Florentin Assanvo. Email: aedjaflorentin@gmail.com

Received: 22 September 2025; Accepted: 19 January 2026; Published: 03 April 2026

ABSTRACT: This study aims to synthesise, characterise and evaluate the performance characteristics of packaging films based on biodegradable natural resources incorporated with nanoparticles. Particularly, it is focused on the valorisation of the fibers from the underexploited *Lonchocarpus cyanescens* plant from West Africa as raw renewable lignocellulose biomass material source for the production of carboxymethylcellulose (CMC). To this end, biodegradable films were prepared from CMC derived from the fibers of the *Lonchocarpus cyanescens* plant, and collagen. In order to improve the properties of these films, in particular their mechanical and humidity resistance and their ability to fight microbes, silver nanoparticles (Ag NPs), titanium dioxide nanoparticles (TiO_2 NPs), as well as heterostructure Ag@TiO_2 nanocomposite were incorporated. The different products obtained were characterised by different methods, including DLS, UV-VIS, SEM, contact angle, UTM, absorption and antimicrobial activity tests. The results show that the hybrid biocomposite films exhibit good mechanical properties, improved moisture resistance, and a significant antimicrobial effect against certain pathogenic bacteria. In particular, the synergy between Ag and TiO_2 nanoparticles in the heterostructure Ag@TiO_2 nanocomposite optimized the performance characteristics of the packaging films, particularly in terms of mechanical properties with a maximum stress of 38.77 MPa and a strain of 9%, low water absorption reaching 50% at 48 h, improved hydrophobic behavior with contact angle of 87°, and antimicrobial resistance compared with the control film without nanoparticles. This work highlights the valorisation of an underexploited West African local plant and contributes to the search for sustainable solutions for food packaging.

KEYWORDS: Biocomposite; carboxymethylcellulose; biodegradable packaging; *Lonchocarpus cyanescens*; heterostructure Ag@TiO_2 nanocomposite

1 Introduction

"What we throw away today could feed tomorrow. What we package today could poison the day after tomorrow". At a time when food security issues are intertwined with global environmental crises [1], one question urgently arises: how can we design materials capable of extending the shelf life of food while disappearing without leaving a trace in nature? Today, more than a third of food produced globally is lost or wasted, or around 1.3 billion tons per year [2]. The main causes of this degradation are well identified: exposure to humidity, oxygen, light, and microbial contamination, particularly during storage and transport. However, packaging is supposed to act as a physical and chemical barrier, and ensure the quality, freshness, safety, and shelf life of food products [3]. Conventional and most efficient synthetic plastic packaging

materials, such as polyethylene or polypropylene are being designed to be resistant to humidity, heat, degradation and unfortunately they permanently pollute the soil, seas and living organisms [4]. According to the report by Atta et al. [5], approximately 300 million tons of plastics are released into the environment each year, of which nearly 50% do not undergo any prior treatment. In addition, poor management of this waste (incomplete incineration or landfill) can lead to the release of toxic substances, harming wildlife and human health. This environmental context is pushing the packaging industry towards the search for alternative, safer and more environmentally friendly materials [5]. This situation has given rise to a new generation of materials: bioplastics and biodegradable films, designed from renewable natural resources and capable of decomposing at the end of their life without negative impact on the environment [6]. Adopting bio-based and biodegradable materials in food packaging offers numerous benefits. These materials reduce plastic pollution, limit dependence on fossil resources, and promote a circular economy. Unlike conventional plastics, they can be naturally degraded or composted, thus reducing their environmental impact [6]. From a functional perspective, some biopolymers exhibit good barrier properties against gases, aromas, or moisture, as well as good suitability for food contact. Furthermore, the choice of suitable materials can help prevent food spoilage by ensuring freshness, slowing oxidation, or inhibiting microbial growth [7]. Additionally, certain polysaccharides such as pectin has been shown to exhibit functional properties like inhibiting lipid absorption, which could be leveraged in active food packaging to improve food quality and safety [8]. Finally, biodegradable materials offer marketing advantages for companies, meeting growing consumer demand for healthier, more sustainable, and environmentally friendly products.

Among the bio-renewable resource based material in packaging, the carboxymethylcellulose, a derived product from cellulose is attracting growing interest in manufacturing biodegradable packaging films due to its biodegradability and biocompatibility, abundance and good film formability, as well as good physical properties [6,9]. The potential properties of CMC leading it a suitable candidate for food packaging including, water solubility, oxygen transfer, fat resistance, high viscosity, and being odorless, tasteless, non-toxic, insensitive, clean, clear [7,10–12], for biomedical applications [13–16] and for support embedded photocatalyst nano-material has emerged as a significant research direction in the field of green materials [8,17]. However, certain limitations, such as brittleness and hydrophilicity, have prompted researchers to explore various approaches to enhance the properties of CMC-based films, making them suitable for food packaging. In this context, chemical modification, nano filler, and physical blending with other bio-polymers have been explored to optimise CMC-based films in food packaging [18,19].

A huge amount of solid wastes containing collagen (Coll) are disposed into the environment from the tanning and related industries, which can be potentially used for the preparation of high-value advanced materials. Coll-based film is considered to be one of the most promising food packaging materials due to its abundant sources, biodegradability, biosafety, self-aggregating and crosslinking, and excellent film-forming capacity [7]. Moreover, the tensile strength of native Coll film with a concentration of 10 mg/mL could reach a good tensile strength of 121 MPa [20]. Additionally, the isoelectric point of Coll protein of pH 7.0 provide Coll-based film the advantage of excellent water resistance [21]. The cationic amino acids and carboxyl groups of Coll can form multiple hydrogen bonds with the anionic carboxyl groups of CMC, and can efficiently integrate through the formation of strong ionic crosslinking interactions, resulting an advanced strong composite film. Therefore, blending CMC with Coll can improve the mechanical property and water resistance [19,20]. Among these cellulose-collagen-based materials films, biocomposite of cellulose-derivated material coupled with Coll have been studied for fully biodegradable food packaging [22–26]. However, the widespread application of the biocomposite collagen-cellulose-based packaging film is currently constrained by challenges including insufficient physicochemical, UV-light barrier and functional characteristics, mechanical stretch, inadequate water and gas resistance, self-antimicrobial and antioxidant,

maintaining freshness. Nanoparticles (NPs) such as Ag NPs, TiO_2 NPs, CuO NPs, ZnO NPs, MgO NPs are commonly used to overcome the above-mentioned disadvantages and promote the application of collagen-cellulose-based biocomposite film in the food packaging [27–29].

While cotton, flax, hemp, jute, kenaf, sisal, ramie, coir, banana, pineapple leaf, bagasse, wheat straw, koffee hull, etc., have been widely valorized and used as cellulose or cellulose derivatives sources in biocomposite materials [30], the use of underutilized local plants is part of an economic, ecological, and rationale strategic priority of Côte d'Ivoire. In West Africa, the *Lonchocarpus cyanescens (L. cyanescens)*, a climbing shrub of the Fabaceae family native to the forests and savannahs, a deciduous plant containing indoxyl is traditionally used as a dye indigo for its pigments. In our previous work, the extracted fiber from the stem of *L. cyanescens* offers a good chemical composition of cellulose (33.3%), hemicellulose (30.3%), and lignin (24.2%) content, exhibits a porous multicellular and polylamellate network structure with a crystallinity index of 56.5% [30]. A comparative analysis of the chemical composition of *L. cyanescens* fiber with other natural fibers is reported in Table 1. The cellulose content (33.3%) with relatively high lignin content (24.2%) suggests that *L. cyanescens* fiber is a good source of cellulose material and resistant to microbial attack, giving its high structural rigidity [30] and potential candidate for the production of bio-based materials.

Table 1: Chemical composition of *L. cyanescens* fiber and comparison with other lignocellulose biomass sources.

Source	Cellulose (%)	Hemicellulose (%)	Lignin (%)	References
Lonchocarpus cyanescens	33.3	30.3	24.2	[30]
Sugarcane bagasse	39.5	23.4	21.0	[30]
Jute	42.5	31.58		[31]
Raw kenaf	45.8	22.8		[31]
Wheat straw	32.8	13.8		[31]
Raw pineapple leaf	57.6	17.26	5.07	[32]
Rice husks	35.6	29.3	20.0	[33]
Corn stover	31.5	18.0	14.1	[31]
Coffee hull	35.5	14.8	30.7	[30]

Herein, it is proposed to isolate cellulose from *L. cyanescens* fibers and its used for the synthesis of CMC. The synthesized CMC is mixed with Coll fibers constituting then the organic matrix and incorporated with Ag NPs and TiO_2 NPs for the formulation of organic-inorganic hybrid food packaging films, with the aim of extending the shelf life of food, while reducing dependence on synthetic polymers, and enhancing local plant resources valorization.

2 Materials and Methods

2.1 Materials

Extracted fibers from *L. cyanescens*, Coll fibers were prepared from the trimmings of cowhides collected from tannery at Central Leather Research Institute, Chennai [34], sulfuric acid (H_2SO_4,), n-octanal (n-C_8H_{16}), anhydrous sodium sulfite (Na_2SO_3), sodium chlorite ($NaClO_2$), sodium monochloroacetic acid (MCAA) ($C_2H_3ClO_2Na$), acetone (C_3H_6O), polyethylene glycol (PEG)($C_2H_6O_2$), nitric acid (HNO_3), titanium(IV) isopropylate (TTIP) ($Ti[OCH(CH_3)_2]_4$), tannic acid ($C_{76}H_{52}O_{46}$), cetyltrimethylammonium bromide (CTAB) ($C_{19}H_{42}BrN$), ethanol (C_2H_6O), silver nitrate ($AgNO_3$), tatanic acid ($C_{76}H_{52}O_{46}$), acetic acid ($C_2H_4O_2$), methanol (CH_4O) and isopropyl alcohol (C_3H_8O). All chemicals were used as received.

2.2 Isolation of Cellulose from the Fiber of L. cyanescens

20 g of dried extracted fiber [30] were boiled with 300 mL of 6% (w/v) hydroxide solution (NaOH) solution for 1 h for the pre-treatment process for the solubilization of surface impurity, hemicellulose, and partially lignin. The pre-treated fiber were washed and ground in a laboratory blender for 5 min to reduce the fiber size (similar to paper pulp). Then, the delignification process was carried out by bleaching with 300 mL of 0.7% (w/v) sodium chlorite under acidic conditions at pH = 4 adjusted with 5% acetic acid solution, and boiled for 3 h. The partially lignin-free fiber residue was washed with distilled water until neutral pH. The neutralized fiber residue was boiled with 300 mL of 5% (w/v) sodium sulfite solution for 5 h to completely remove lignin as well as partially remove of hemicellulose. The obtained holocellulose was boiled with 300 mL of 17.5% (w/v) NaOH solution for 5 h to remove hemicelluloses. The isolated cellulose was washed with distilled water until neutral pH and air-dried.

2.3 Preparation of Ag NPs

In a 500 mL round flask, 170 mL of distilled water and 10 mL of 0.1 M CTAB solution were stirred for 10 min at 30°C. To this solution, 10 mL of 0.1 M silver nitrate solution was added dropwise with continuous stirring for 10 min. 20 mL solution of water containing 1.4 g of previously dissolved tannic acid was added to initiate the reduction reaction. The color of the solution changed from colorless to yellowish brown. After adding a few drops of NaOH solution (0.1 M), the color of the solution changed to dark brown and the reaction was stirred at room temperature for 2 h. The mixture was centrifuged at 15.000 rpm for 15 min at 4°C. The residue was washed three times with distilled water and once with ethanol. The Ag NPs were dried in an air oven at 80°C for 4 h.

2.4 Preparation of TiO_2 NPs

For the synthesis of TiO_2 nanoparticles, 5 mL TTIP was introduced into 20 mL of ethanol, and then the mixture was stirred at 500 rpm at a temperature of 60°C for 30 min. Next, a mixture composed of 20 mL of ethanol and distilled water (1:1) (v/v) was prepared, and then 2 mL of concentrated nitric acid (72%) was added dropwise under constant stirring. This mixture was gradually incorporated into the first solution, and the whole was stirred at 1000 rpm for 3 h at 100°C, which led to the formation of a gel. The obtained product was centrifuged at 10,000 rpm for 20 min. The precipitate was collected, washed successively with distilled water and then with ethanol to remove residual impurities. After drying at 100°C for 8 h in a hot air oven, the dried powder was calcined at 500°C for 2 h under nitrogen atmosphere to obtain TiO_2 NPs.

2.5 Preparation of the Heterostructure Ag@TiO_2 Nanocomposite

The preparation of the heterostructure Ag@TiO_2 nanocomposite was carried out according to the following protocol: a reaction mixture with a ratio of 1:0.2 of TTIP and Ag NPs was used. Briefly, 0.24 g of Ag NPs was dissolved in 10 mL of ethanol and stirred at 500 rpm for 10 min. Then, 1.2 g of TTIP was added dropwise to the above mixture and the reaction continued for 1 h 30 min at 60°C. The resulting colloidal solution was transferred to a crucible and dried at 55°C for 24 h, then calcined at 450°C for 2 h under nitrogen purge.

2.6 Synthesis of CMC from L. cyanescens Fibers

CMC was synthesized from cellulose extracted from *L. cyanescens* according to the method described by [9]. The synthesis reaction of CMC proceeds in two steps: alkalization, followed by etherification of cellulose under heterogeneous conditions. First step: 1 g of isolated cellulose powder was introduced into 100 mL Erlenmeyer flask, and 60 mL of water-isopropanol alcohol solvent mixture of ratio (1:4) was added.

Alkalization was carried out by dropwise addition of 8 mL of NaOH solution at different concentrations (10%, 20%, 30% and 40%) (w/v) under magnetic stirring for 2 h at room temperature (~30°C). Afterwards in the second step, the carboxymethylation reaction was initiated by adding a variable amount of MCAA (0.4; 0.8; 1.2; 1.6 g) to the reaction mixture. The mixture was heated at 60°C under reflux and continuous magnetic stirring for 3 h. Then the precipitate was separated by filtration and placed in 100 mL of methanol for 40 min. Finally, a quantity of glacial acetic acid was added to neutralize the mixture. Then filtered and washed four times with 50 mL of 80% ethanol. To remove unwanted salts, the mixture was washed again with 50 mL of absolute methanol. The final product was dried in an air dryer at 50°C for 12 h. The recipe for the experiments (CMC1, CMC2, CMC3 and CMC4) of the synthesis of CMCs is summarized in Table 2.

Table 2: Recipe for CMC formulation.

Reagents	Experiments			
	CMC1	**CMC2**	**CMC3**	**CMC4**
NaOH	10%	20%	30%	40%
MCAA (g)	0.4	0.8	1.2	1.6

The yield (%) of CMC is calculated according to the following relationship:

$$CMC\,(\%) = \frac{Weight\ of\ CMC\ (g)}{Weight\ of\ cellulose\ (g)} \times 100 \quad (1)$$

2.7 Formulation of Organic-Inorganic Collagen-Carboxymethylcellulose (Coll-CMC)-Nanoparticles (Coll-CMC-NPs) Hybrid Composite Films

In 100 mL beaker, 0.7 g of CMC based on *L. cyanescens* fiber was dissolved in 30 mL of distilled water under magnetic stirring of 1000 rpm at 80°C for 1 h. Meanwhile, in another 100 mL beaker, 0.3 g of Coll was also dissolved in 20 mL of 0.5 M acetic acid solution with an Ika homogenizer for 10 min. The formulation of the bioplastic was carried out by adding the Coll solution dispersion to the CMC solution at room temperature with 10% of PEG as a plasticizer and emulsifier to reduce crystallinity and improve the mechanical properties and thermal stability [35]. The mixture was stirred at 1200 rpm for 2 h. For the preparation of hybrid composite films, 5% of nanoparticles was added to the organic mixture. The homogeneous plastic product was cast into a plastic Petri dish and dried at room temperature for 24 h, and then at 40°C in an air oven for 30 min to obtain an organic-inorganic hybrid film. Table 3 summarizes the recipe for the experiments (Formulation 1, Formulation 2, Formulation 3 and Formulation 4).

Table 3: Recipe for the formulation of hybrid nanocomposite films.

Reagents (%)	Experiments			
	Formulation 1	**Formulation 2**	**Formulation 3**	**Formulation 4**
Coll	30	30	30	30
CMC	70	70	70	70
PEG	10	10	10	10
TiO_2 NPs	0	5	0	0
Ag NPs	0	0	5	0
Ag@TiO_2 nanocomposite	0	0	0	5

2.8 Preparation of Spore and Bacterial Solution

The pathogenic bacterial strains (*Staphylococcus aureus, Bacillus cereus and Salmonella typhi*) previously stored at −80°C were recovered and cultured on a nutrient agar for bacteria. The agar was then incubated in an incubator at 37°C for 24 h in order to obtain young and viable cells. Then, the revived strains were cultured in a nutrient broth. The culture broth was subsequently incubated at 37°C for 24 h. The load of the obtained cultures was adjusted to 107 cell/mL using a spectrophotometer according to the method [36]. The antibacterial tests were conducted under direct solar light condition.

2.9 Characterizations

The Dynamic Light Scattering (DLS) was used to determine the average hydrodynamic diameter of the synthesized nanoparticles. Measurements were performed using a Litesizer 500 particle analyzer.

The UV-visible spectra of the nanoparticles were obtained using a UV-visible spectrophotometer (Shimadzu UV-1800). The spectrum was taken from 0 to 800 nm with a scanning interval of 0.5 nm.

The surfaces of the samples were analyzed using a scanning electron microscope field emission spectroscopy (FESEM, TESCAN, model-CLARA) operating at an accelerating voltage of 15.0 kV. Prior to SEM observation, the samples were sputtered with a thin layer of gold to avoid the charging effects of the electron beam during examination.

The degree of substitution (DS) of CMC from *L. cyanescens* fibers represents the average number of hydroxyl groups replaced by carboxymethyl and sodium carboxymethyl groups at C2, C3, and C6 in the cellulose structure. The DS was determined by titration according to ASTM-D1439-03 standard.

The mechanical properties of the composite films were determined using a Universal Testing Machine (UTM) (Zwick/Z010) in accordance with ASTM D638. All experiments were carried out at a cross-sectional speed of 5 mm/min with an initial length L0 of 140 mm. The tensile strength and elongation at break measurements were carried out with three (03) repetitions for each sample and the average value was recorded.

The contact angle of the synthesized films was determined using the sessile drop method using a Drop Shape Analyzer—DSA25 equipped with a monochrome camera B-CAM-21-BW (CCCIR) and an LED R60 lamp (Conrad). 4 µL of distilled water was deposited on the surface of each film and the contact angle was recorded after 30 s. One Touch Grabber and Image J software were used to calculate the contact angles. An average value was obtained for triplicate measurements.

The water absorption behavior of the synthesized film samples was examined by gravimetric method as reported by [37], then adapted to our study. Indeed, samples of film were cut into squares measuring 1 cm × 1 cm and mass m_0 previously known were immersed in 50 mL of distilled water, at room temperature for 48 h. Every 4 h the samples were removed from the water, cleaned using paper to remove excess residual water on the surface and weighed (m_1). Finally, the water absorption rate of samples was determined as follows:

$$water \text{ absorption rate } (\%) = 100 \times \frac{m_1 - m_0}{m_0} \quad (2)$$

The absorption rate retained is the average of three values measured on 3 samples, for each formulation.

The demonstration of antibacterial activity was carried out according to the method recommended by Barefoot and Klaenhammer [38]. The Mueller-Hinton agar was prepared according to the manufacturer's instructions and sterilized at 121°C for 15 min. The prepared media were poured into Petri dishes. After solidification, a volume of 100 µL of the microbial suspension (107 spores/mL) prepared previously was deposited on the surface of the agar and then spread. Film discs of 1 cm in diameter were placed on the agar

which had been previously inoculated with the pathogenic strain. The Petri dishes were placed at 4°C for 1 h to allow good diffusion of the antimicrobial substance. The dishes were then incubated at 37°C. The presence of inhibition zones formed around the discs was examined after 24 h of exposure in solar light [39].

3 Results and Discussion

3.1 Determination of Particles Sizes

The average particle size and distribution size of TiO_2 NPs, Ag NPs, and heterostructure Ag@TiO_2 nanocomposite are shown in Fig. 1. The measured sizes are 46, 140, and 403 nm for TiO_2 NPs, Ag NPs, and Ag@TiO_2 nanocomposite, respectively. These results show that TiO_2 NPs are the smallest and most uniform. The Ag NPs exhibit a slightly broader distribution with relatively large size. In contrast, the particle size of Ag@TiO_2 nanocomposite is significantly larger, with a broader particle size distribution, indicating that the particles are probably agglomerated. It has been reported the size-dependent antibacterial efficacy of nanoparticles [40–44]. The antibacterial efficacy increases with the decreasing particles size. Beyond size, shape-dependent also plays an important role in the antibacterial performance of Ag NPs [40]. Ali et al. [45] compared antibacterial efficacy of Ag NPs, TiO_2 NPs and Ag@TiO_2 nanocomposite against *Escherichia Coli, Pseudomonas aeruginosa, Klebsiella pneumoniae and Enterobacter Cloacae*. The authors concluded that, the heterostructure Ag@TiO_2 nanocomposite show enhanced antibacterial activity against bacterial strains because of its high surface area and best against bacterial adhesion lead to higher reactivity and releases high amount of Ag^+ than that from Ag NPs and TiO_2 NPs [41,44,45].

3.2 UV-Visible Analysis

The UV-visible absorption spectra of the synthesized nanoparticles (TiO_2, Ag and Ag@TiO_2) are plotted in Fig. 2. The spectrum of TiO_2 NPs shows an absorption band in the ultraviolet, with a maximum around 340 nm, characteristic of the electronic transitions of the anatase TiO_2 semiconductor [46]. This property is important for photocatalytic application, as it allows TiO_2 NPs to act as a self-cleaning or decontaminating agent under UV radiation [46]. Ag NPs, for their part, present a marked absorption peak around 420 nm, attributed to surface plasmon resonance (SPR) [47]. This optical phenomenon results from the collective vibration of electrons on the surface of the nanoparticles when exposed to light. The presence of this characteristic peak indicates that the Ag NPs are well formed. In addition, the position and intensity of this SPR peak provide important information on the relatively large size and non-agglomeration of the prepared Ag NPs, two essential elements to evaluate their antibacterial efficacy [47,48]. The spectrum of the heterostructure Ag@TiO_2 nanocomposite shows both signatures, an absorption in the UV (inherited from TiO_2 NPs), and a broadening of the absorption in the visible around 420 nm (related to Ag NPs). This superposition confirms that the Ag NPs have been well grafted onto the surface of the TiO_2 NPs, forming a heterostructure nanocomposite. The introduction of Ag NPs causes a red shift of the UV-visible spectra edges to longer wavelength compared to pristine TiO_2. The shift in the absorption of TiO_2 is favourable for the improvement of photocatalytic and photo-oxidized activities of TiO_2 under both UV and visible regions and expands the antimicrobial activity of Ag@TiO_2 nanocomposite response range under direct solar condition. The band gap of TiO_2 (~3.2 eV) is higher than that of Ag (~2.25 eV) leading to reducing the band gap of the heterostructure Ag@TiO_2 nanocomposite (~2.2–2.9 eV) [43,49] and promoting the transfer of electrons from valence band (VB) to the conduction band (CB). Because, the Ag CB is below the TiO_2 CB, while the Ag VB band is above the TiO_2 VB band. Consequently, when the heterostructure Ag@TiO_2 nanocomposite is exposed to solar light, electrons (e-) migrate from the CB of TiO_2 to the CB of Ag, while holes (h+) are transfer from the VB of TiO_2 to the VB of Ag preventing the reduction of electrons recombination as illustrated by the scheme in Fig. 3. The electron–hole pairs generated take part in a series of oxidation/reduction reactions

with species adsorbed on the TiO_2 surface, to generate highly reactive oxygen species (ROS). Ag@TiO_2 nanocomposite exhibits enhanced ROS formation activity under visible light compared to pristine TiO_2, due to the SPR effect of Ag NPs [50]. ROS are natural by-products of cellular oxidative metabolism and play important roles in the modulation of cell survival, cell death, differentiation, cell signaling [50,51]. Thus, the photocatalytic activity of Ag@TiO_2 nanocomposite increases the level of ROS in the bacteria cells and disrupts the cellular oxidative metabolism, consequently, the cells endure very high oxidative stress that leads to the death of the bacteria. This type of assembly is known to be more stable and more effective against microbes, thanks to the combined action of TiO_2 NPs, which destroys germs with light, and Ag NPs, which kills microorganisms [48]. Thus, the UV-Visible results confirm the quality of the synthesized nanoparticles and validate their suitability for use in biodegradable functional films for food applications as antimicrobial.

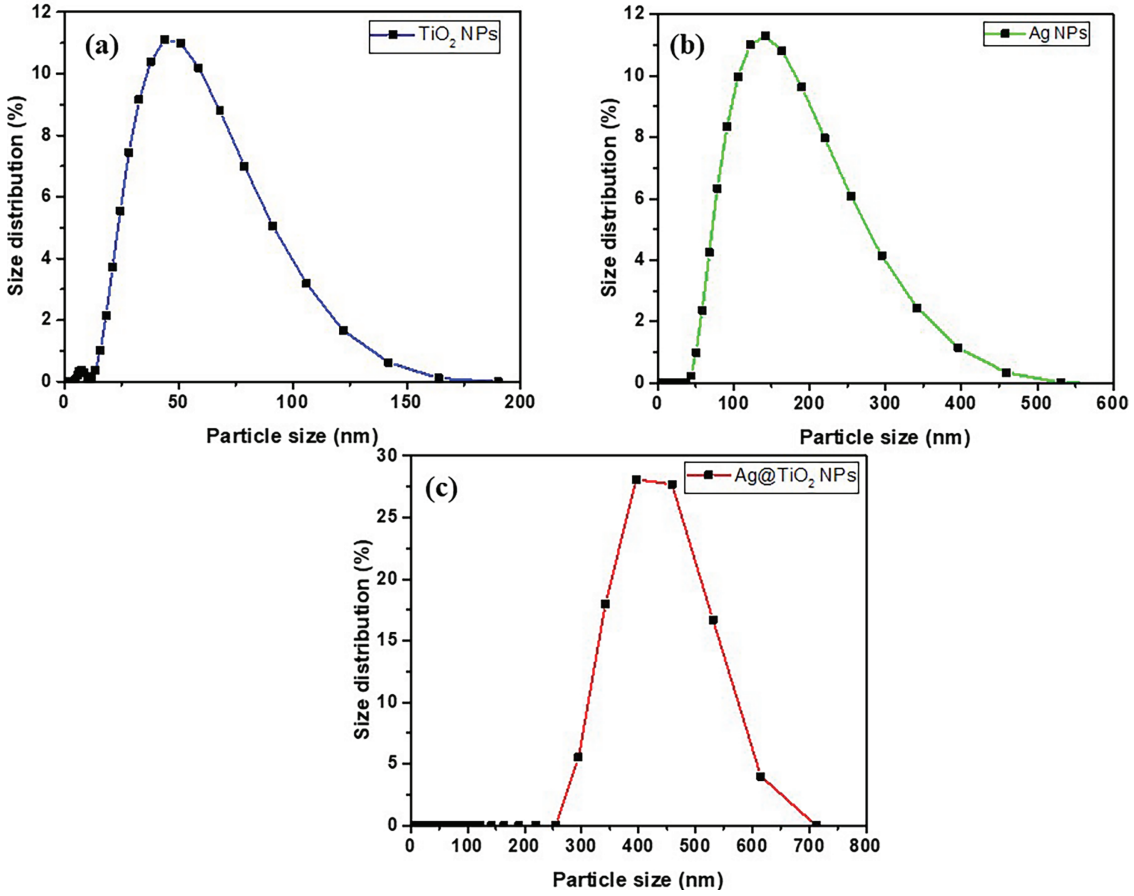

Figure 1: Particles size and distribution curves of (**a**): TiO_2 NPs, (**b**): Ag NPs and (**c**): Ag@TiO_2 NPs.

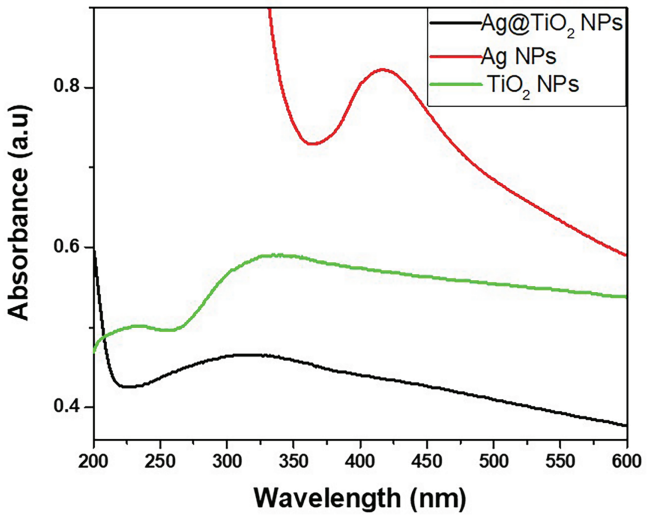

Figure 2: UV-visible absorption spectra of TiO_2 NPs, Ag NPs and Ag@TiO_2 NPs.

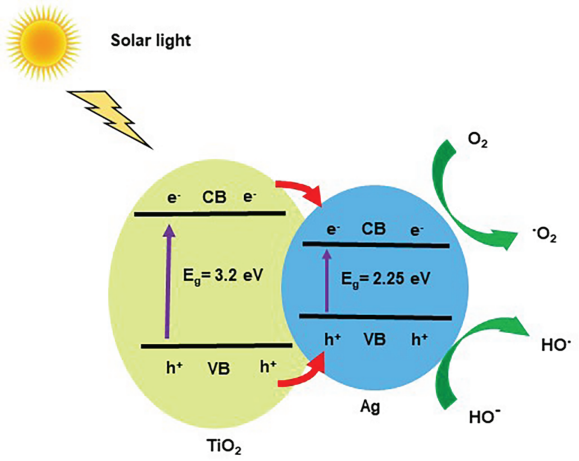

Figure 3: Schematic diagram representing the photocatalytic degradation mechanism of heterostructure Ag@TiO_2 nanocomposite.

3.3 Percentage Yield and Degree of Substitution (DS) of CMC

The percentage yield of the synthesized CMC is presented in Fig. 4a and shows a characteristic evolution as a function of NaOH concentration. Indeed, the yield of CMC increases significantly when the NaOH concentration increases from 10% to 30% reaching a maximum of 91% for CMC3, before decreasing to 77% at the NaOH concentration of 40%. This phenomenon resulting from the decrease in CMC yield could be due to a limitation of MCAA as an etherifying agent to replace the OH groups of cellulose. The DS exhibits the same trends with the NaOH concentration (Fig. 4b) with the maximum of 0.95 at 30% of NaOH concentration. Thus, the 30% NaOH concentration seems to be an optimal balance point to obtain a high yield while maintaining the structural integrity of the modified cellulose. This behavior is explained by two reactions that occur simultaneously during the carboxymethylation process. The first (Eq. (2)) involves the reaction of a hydroxyl group of cellulose with MCAA in the presence of NaOH, which leads to the formation of CMC. The second, concurrent and unwanted, consists of the reaction between NaOH and MCAA, forming

a by-product called sodium glycolate according to the equation:

$$NaOH + Cl\text{-}CH_2COONa \rightarrow HO\text{-}CH_2COONa + NaCl \quad (3)$$

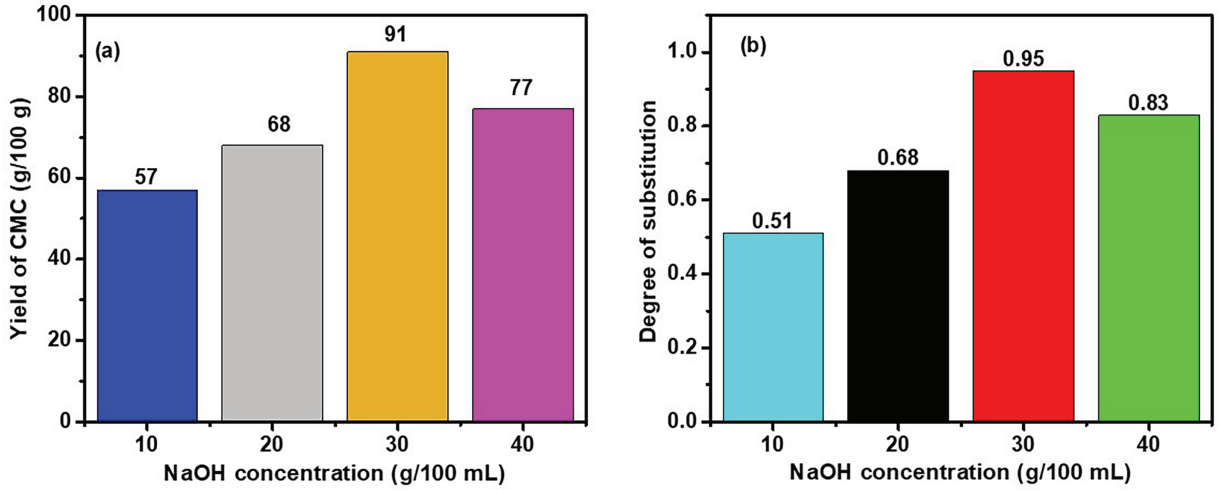

Figure 4: (**a**): CMC yield and (**b**): DS as function of NaOH concentration.

When the sodium hydroxide concentration is too high, this secondary reaction becomes dominant and consumes MCAA, thus reducing the amount available for the main reaction and resulting in the decreasing of the DS. This phenomenon was confirmed by the results of Joshi et al. [52].

3.4 Morphological Analysis of Films

The photographs and SEM morphological observation images of the films in Fig. 5 show a clear influence of the nature of the nanoparticles on the appearance and the surface morphology of films. The control film (Fig. 5a) without nanoparticles appears white and presents a smooth and homogeneous surface. The introduction of TiO_2 NPs (Fig. 5b) generates a yellowish film with a slight roughness and fine aggregates well integrated into the matrix, while the dark glossy black film with Ag NPs in Fig. 5c exhibits strong roughness with random dispersion and distribution of Ag NPs particles sizes on the surface. In contrast, the film containing the heterostructure Ag@TiO_2 nanocomposite (Fig. 5d) reveals a heterogeneous black with a white tone surface appearance marked by massive agglomerates, a sign of less efficient dispersion. These morphological differences suggest that the incorporation and type of nanoparticles strongly influence the microscopic structure of the films, which could affect their functional properties such as mechanical strength, permeability and antimicrobial activity.

3.5 Contact Angle Measurement

The results of the water contact angles of the films are illustrated by the images presented in Fig. 6. The measured angles are 53°, 62°, 71° and 87° respectively for formulation 1, formulation 2, formulation 3 and formulation 4. A progressive increase in the contact angle from 53° to 87° is observed, reflecting a decrease in wettability and an increasing trend towards hydrophobicity. The film (Fig. 6a) without nanoparticles exhibits the lowest contact angle (53°), indicating strong hydrophilicity attributed to CMC, a naturally hydrophilic polymer. The addition of TiO_2 NPs and Ag NPs in formulation 2 and formulation 3 (Fig. 6b,c, respectively) significantly the contact angle, suggesting a reduction in wettability due to a change in surface roughness.

Formulation 4, containing heterostructure Ag@TiO_2 nanocomposite reaches a maximum angle of 87° as shown in the Fig. 6d and close to hydrophobic behavior. It has been reported that the synergetic effect of bimetallic in collagen-cellulose sponge increases the water angle up to 123° [53]. Upon immobilizing collagen within the bacterial cellulose matrix via tannin, the water contact angle increased further due to the formation of hydrogen bonds between cellulose fibers, collagen, and tannin, reducing then the numbers of free hydroxyl groups with increase in the hydrophobicity of the composite film [19]. These results show a conformity with those obtained by the DLS test where the particle size increases with the surface roughness which is important for food packaging applications where a certain resistance to humidity is sought.

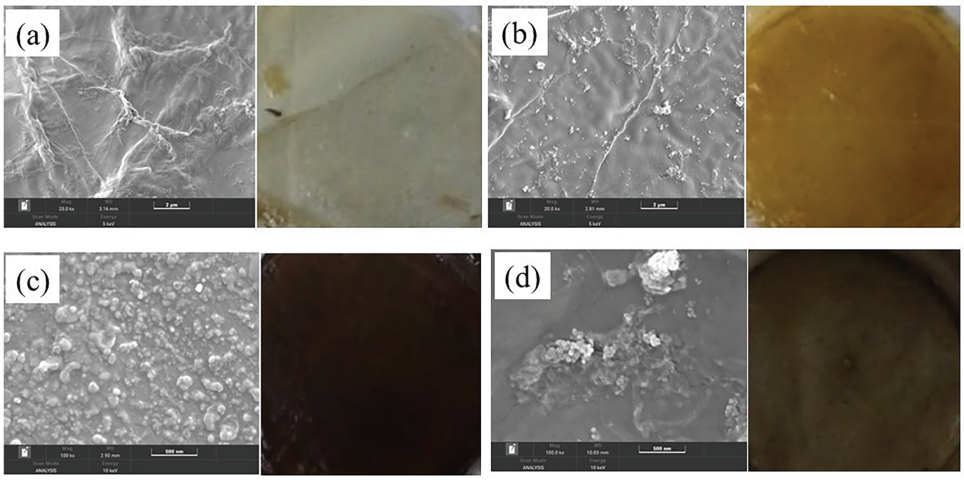

Figure 5: Photographs and SEM images of biocomposite films (**a**): without NPs, (**b**): with TiO_2 NPs, (**c**): with Ag NPs and (**d**): with Ag@TiO_2 nanocomposite.

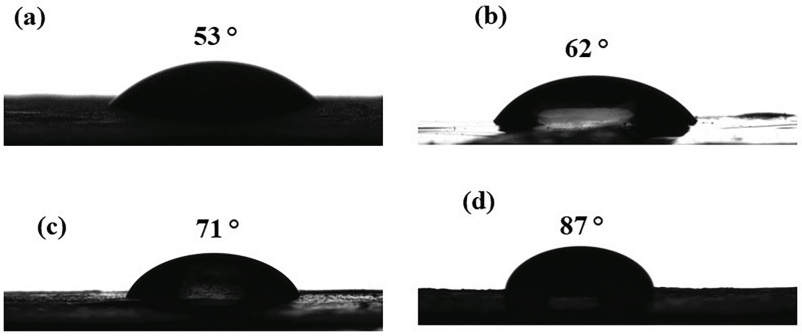

Figure 6: Images of water contact angles of films (**a**): Control, (**b**): with TiO_2 NPs, (**c**): with Ag NPs and (**d**): with Ag@TiO_2 nanocomposite.

3.6 Mechanical Properties

Fig. 7 illustrates the stress-strain curves obtained from the tensile tests on the biocomposite films (formulation 1 to formulation 4). In general, all the curves show a progressive increase in stress with deformation, until reaching a maximum value followed by a sudden rupture. This behavior indicates a certain capacity of the films to deform before rupture [54]. The control film (Control), free of nanoparticles, shows the lowest performance with a maximum stress of 9.08 MPa and a strain of 1.77%, reflecting low mechanical strength and limited elasticity. The addition of TiO_2 NPs leads to a significant improvement in mechanical

properties, with the stress of 30.78 MPa and strain of 7.17%, which can be attributed to a good reinforcing effect of inorganic fillers in the polymer matrix [55]. The formulation 3 film containing only Ag NPs, shows an even higher strength (31 MPa) but a reduced strain (2.03%), suggesting brittleness of the material. This low strain could be explained by the agglomeration of Ag NPs in the matrix, leading to poor load distribution and the formation of stress concentration zones [56]. On the other hand, the formulation 4 film containing the Ag@TiO_2 nanocomposite, shows the best mechanical performance with a maximum stress of 38.77 MPa and a strain of 9% characteristic of a ductile material. This notable improvement can be interpreted as the result of a synergistic effect between the Ag NPs and TiO_2 NPs, allowing both a good load transfer, a reinforced interaction with the matrix and a better homogeneity in the load distribution [48]. These results confirm the interest of this hybrid biocomposite for packaging applications, where the combination of strength and flexibility is essential.

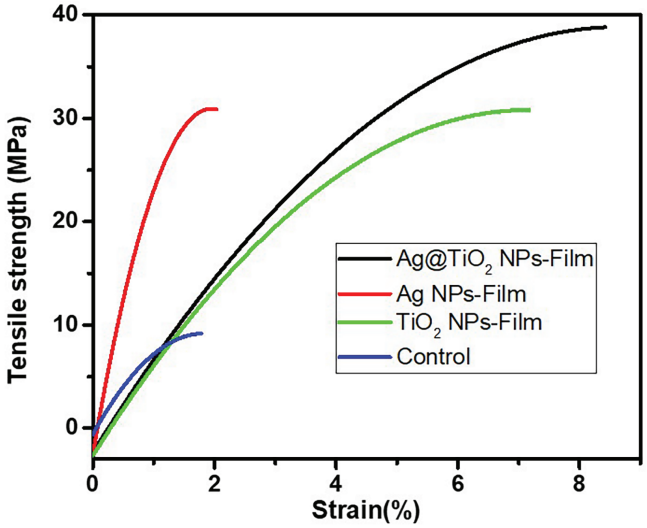

Figure 7: Stress-strain curve of biocomposite films.

3.7 Water Absorption

The kinetic study of water absorption of the different formulated films is illustrated in Fig. 8 and shows a characteristic two-phase evolution: an initial phase of rapid absorption followed by a plateau, reflecting the progressive saturation of the hydrophilic sites of the polymer matrix. The control film, formulation 1 composed of the organic matrix Coll-CMC, displays the highest water absorption capacity, almost 100% at 48 h. This behavior is attributable to the intrinsic hydrophilic nature of CMC, rich in hydroxyl groups, promoting water retention by hydrogen interactions and swelling of the macromolecular network [57–60]. The distribution pattern of the interconnected Coll and CMC formed three-dimensional structures and Coll fibrils tend to penetrate the CMC network to form a supramolecular double network structure composite material [60]. The high water absorption could be explain by the loose network structure of Coll fibrils within the composite. The introduction of inorganic nanoparticles into the organic matrix significantly affects the absorption kinetics and capacity. The formulation 2 film containing TiO_2 NPs, shows a notable reduction in the absorption rate to 80% at 48 h. This decrease is explained by the barrier effect created by the nanoparticles, which partially fill the pores and limit the diffusion of water into the matrix. In addition, the interactions between the hydroxyl groups of the CMC and the polar surfaces of TiO_2 contribute to a densification of the network, as highlighted by [29] in chitosan-based films reinforced with TiO_2. The formulation 3 film enriched with Ag NPs, reaches a maximum absorption of 65%. This intermediate value suggests that Ag NPs, although

less effective than TiO_2 NPs as a physical barrier, nevertheless interact with the Coll-CMC matrix. These interactions (coordinated bonds or hydrogen bonding with the carboxylate groups) slightly limit the chain mobility and the availability of active sites for water adsorption. These effects have been reported by [47] who studied the modification of Ag NPs-based films in active packaging applications. Finally, the formulation 4 film containing the heterostructure $Ag@TiO_2$ nanocomposite shows the lowest water absorption, reaching 50% at 48 h. This result is consistent with a dual action: on the one hand, the dense and hydrophobic structure induced by the presence of TiO_2 NPs; on the other hand, the synergistic effects of Ag NPs that reinforce the cohesion of the matrix by the release of the metal ion Ag^+ to formed intramolecular metal-ligand bonds stable to water in wet heterostructure $Ag@TiO_2$, nanocomposite [60]. Such synergy has been documented by Akhavan [48] in Ag/TiO_2 hybrid systems embedded in polysaccharide matrices, showing a significant reduction in water permeability and an improvement in dimensional stability. Kinetically, it is observed that the nanoparticle-loaded films reach their absorption plateau more slowly than the Coll-CMC film alone, indicating a slower diffusion of water within the reinforced organic matrices. This dynamics can be modeled by pseudo-first-order kinetics, suggesting that the imbibition rate is controlled both by water diffusion in the pores and by the availability of active sites on the surface of the polymer chains. In conclusion, the results obtained clearly show that the incorporation of nanoparticles, particularly the heterostructure $Ag@TiO_2$ nanocomposite can effectively reduce the hydrophilicity of Coll-CMC-based films. This strategy is promising for the formulation of barrier films for food, biomedical or smart packaging applications, where water resistance is crucial.

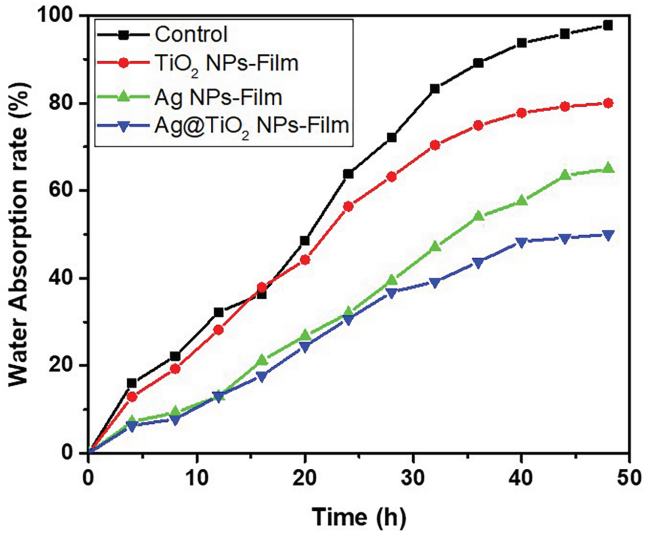

Figure 8: Water absorption rate curves of biocomposite films.

3.8 Antimicrobial Properties

The standard disk diffusion method was used to evaluate the antibacterial activity of TiO_2 NPs, Ag NPs, and heterostructure $Ag@TiO_2$ nanocomposite against three bacterial strains. Fig. 9 displays the results of the test. Among the tested samples, heterostructure $Ag@TiO_2$ nanocomposite showed the most pronounced antibacterial effect on all bacteria. In contrast, TiO_2 NPs alone did not show a significant inhibition zone. This low efficacy could be attributed to their relatively smaller size, as reported by [61]. The significant improvement in antibacterial activity in the case of the $Ag@TiO_2$ nanocomposite could result from a synergistic effect between the Ag NPs and the TiO_2 NPs. Indeed, the presence of Ag NPs would amplify the antibacterial effect, in particular thanks to the increase in the size of the particles in the composite, promoting

better interaction and adhesion with bacterial cells [61]. This enhanced activity can be explained by several mechanisms. On the one hand, the release of metal ions (especially Ag^+) from the surface of nanoparticles would contribute to toxicity towards microorganisms. On the other hand, the generation of reactive oxygen species (ROS) would play a key role, particularly in the case of TiO_2 NPs, which triggers a photocatalysis process under natural sunlight irradiation and releases hydroxyl radicals (OH) and superoxides (O_2-) in an aqueous medium. These ROS attack cell membranes by degrading phospholipids and can also induce damage to bacterial DNA, leading to a pronounced antibacterial effect as mentioned earlier.

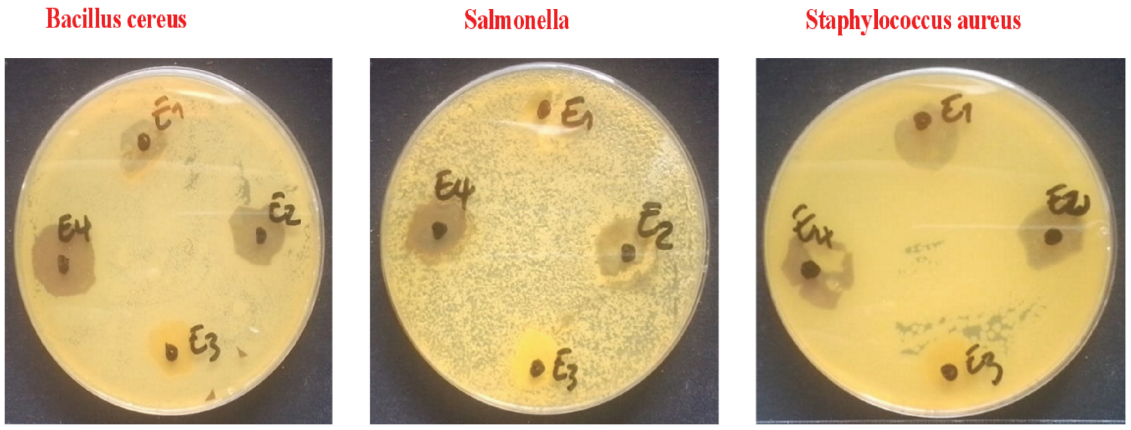

Figure 9: Results of disk diffusion test of E1: Control, E2: TiO_2 NPs, E3: Ag NPs and E4: Ag@TiO_2 nanocomposite.

4 Conclusions

This present study explored the synthesis and characterisation of biodegradable biocomposite films, offering an ecological alternative to conventional plastic packaging, responsible for lasting pollution. The work focused on the formulation of films based on CMC synthesised from fibers extracted from *Lonchocarpus cyanescens*, an underexploited local plant from Côte d'Ivoire in West Africa. To improve their properties, nanoparticles of silver (Ag), titanium dioxide (TiO_2), as well as heterostructure Ag@TiO_2 nanocomposite have been incorporated. The obtained nanoparticles and biocomposite films were subjected to various characterisations, including DLS, UV-VIS, SEM, water contact angle and UTM analyses, as well as water absorption and antimicrobial activity tests. The as-prepared nanoparticles show particles of 46, 140, and 403 nm for TiO_2 NPs, Ag NPs, and Ag@TiO_2 nanocomposite, respectively, with relatively low distribution. The maximum yield of the CMC is 91% at 30% of NaOH concentration. From the SEM observations, it is found that the nature and type of nanoparticles effluent the morphology of the formulated films, ranging from smooth surface to rough. The incorporation of nanoparticles in the formulation has significantly improved the performance characteristics of the packaging film, including good mechanical properties, improved moisture resistance and a notable antimicrobial effect against certain pathogenic bacteria (*Staphylococcus aureus, Bacillus cereus and Salmonella typhi*). In particular, the synergy of Ag and TiO_2 nanoparticles within the heterostructure Ag@TiO_2 nanocomposite made it possible to optimise the antimicrobial performance of the films. Future research will be carried out to fully characterise the CMC based on the fiber in terms of molecular weight, and also the optimisation of the preparation of the hybrid packaging film and its direct application for food packaging.

Acknowledgement: The author feel thankful to CSIR-Central Leather Research Institute (CLRI), Chennai, India where the laboratory experiments have been done, and the President of University Nangui Abrogoua, Abidjan, Côte d'Ivoire.

Funding Statement : This research was funded by CSIR-TWAS Postdoctoral Fellowship grand number FR 3240316961.

Author Contributions: Edja Florentin Assanvo: conception, design, experimental investigation and data collection, writing the initial draft, revising the manuscript. N'Dri N'Guessan Gervais Ziabo: data interpretation and analysis, visualization and contributed to writing and revision. Kohi Alfred Kouame: antimicrobial analysis and interpretation. David Boa: supervision and checked the manuscript for improvement. All authors reviewed and approved the final version of the manuscript.

Availability of Data and Materials: The data that support the findings of this study are available from the corresponding author, EFA, upon reasonable request.

Ethics Approval: Not applicable

Conflicts of Interest: The authors declare no conflicts of interest.

References

1. Amand MAV, Wang W-L, Yang C-J, Lai J-Y, Yao C-H. Snails as a multifunctional biological resource: nutritional value and pharmacological applications. Food Res Int. 2026;223(2):117872. doi:10.1016/j.foodres.2025.117872.
2. Blakeney M. Food loss and food waste: causes and solutions. Cheltenham, UK: Edward Elgar Publishing; 2019. doi:10.4337/9781788975391.
3. Haghighi H, Licciardello F, Fava P, Wilhelm H, Pulvirenti A. Recent advances on chitosan based films for sustainable food packaging applications. Food Packag Shelf Life. 2020;26(8):100551. doi:10.1016/j.fpsl.2020.100551.
4. Groh KJ, Backhaus T, Carney-Almroth B, Geueke B, Inostroza PA, Lennquist A, et al. Overview of known plastic packaging-associated chemicals and their hazards. Sci Total Environ. 2019;651(2):3253–68. doi:10.1016/j.scitotenv.2018.10.015.
5. Atta OM, Manan S, Ahmed AAQ, Awac MF, Ul-Islam M, Subhan F, et al. Development and characterization of yeast-incorporated antimicrobial cellulose biofilms for edible food packaging application. Polymers. 2021;13(14):2310. doi:10.3390/polym13142310.
6. Yaradoddi JS, Banapurmath NR, Ganachari SV, Soudagar MEM, Mubarak NM, Hallad S, et al. Biodegradable carboxymethyl cellulose based material for sustainable packaging application. Sci Rep. 2020;10(1):21960. doi:10.1038/s41598-020-78912-z.
7. Shi X, Ju F, Wang R, Xu J, Li T, Wei T, et al. Brilliant fabrication of multifunctional collagen-based packaging films with rigid-flexible coupling structure bio-inspired by pangolins. Food Chem. 2025;479(6):143814. doi:10.1016/j.foodchem.2025.143814.
8. Liu F, Zhu K, Ma Y, Yu Z, Chiou B-S, Jia M, et al. Collagen films with improved wet state mechanical properties by mineralization. Food Hydrocoll. 2023;139(2):108579. doi:10.1016/j.foodhyd.2023.108579.
9. Wang X, Liu Y, Xu Y, Gao S, Xu Q, Gong H, et al. Structural characterization of a pectic polysaccharide from Rubus chingii Hu. unripe fruits and its efficacy in inhibiting intestinal lipid absorption *in vivo*. Carbohydr Polym. 2025;363(1):123728. doi:10.1016/j.carbpol.2025.123728.
10. Roy S, Kim H-J, Rhim J-W. Synthesis of carboxymethyl cellulose and agar-based multifunctional films reinforced with cellulose nanocrystals and Shikonin. ACS Appl Polym Mater. 2021;3(2):1060–9. doi:10.1021/acsapm.0c01307.
11. Zhao G, Lyu X, Lee J, Cui X, Chen W-N. Biodegradable and transparent cellulose film prepared eco-friendly from durian rind for packaging application. Food Packag Shelf Life. 2019;21(36):100345. doi:10.1016/j.fpsl.2019.100345.
12. Klunklin W, Jantanasakulwong K, Phimolsiripol Y, Leksawasdi N, Seesuriyachan P, Chaiyaso T, et al. Synthesis, characterization, and application of carboxymethyl cellulose from asparagus stalk end. Polymers. 2021;13(1):81. doi:10.3390/polym13010081.
13. Ramakrishnan R, Kim JT, Roy S, Jayakumar A. Recent advances in carboxymethyl cellulose-based active and intelligent packaging materials: a comprehensive review. Int J Biol Macromol. 2024;259(1):129194. doi:10.1016/j.ijbiomac.2023.129194.
14. Zhong N, Cao N, Cheng Z, Fang S, Jiang M, Guan J, et al. Enhanced carboxymethyl cellulose based hydrogels for wound dressings. ACS Appl Bio Mater. 2025;8(7):5532–46. doi:10.1021/acsabm.5c00815.

15. Almasian A, Najafi F, Eftekhari M, Ardekani MRS, Sharifzadeh M, Kjanavi M. Polyurethane/carboxymethylcellulose nanofibers containing Malva sylvestris extract for healing diabetic wounds: preparation, characterization, *in vitro* and *in vivo* studies. Mater Sci Eng C. 2020;114(2):111039. doi:10.1016/j.msec.2020.111039.
16. Kanikireddy V, Varaprasad K, Jayaramudu T, Karthikeyan C, Sakiku R. Carboxymethyl cellulose-based materials for infection control and wound healing: a review. Int J Biol Marcomol. 2020;164:963–75. doi:10.1016/j.ijbiomac.2020.07.160.
17. Wang F, Zhang Q, Huang K, Li J, Wang K, Zhang K, et al. Preparation and characterization of carboxymethyl cellulose containing quaternized chitosan for potential drug carrier. Int J Biol Marcomol. 2020;154(4):1392–9. doi:10.1016/j.ijbiomac.2019.11.019.
18. Patel AK, Kawale AP, Sharma N, Sheckar N, Banerjee S, Srivastava A. Synthesis and characterization of CMC-wrapped ZnO NPs at different calcination temperatures for photocatalytic degradation of methylene blue dye under sunlight. J Polym Mater. 2024;41(2):69–86. doi:10.32604/jpm.2024.052695.
19. Nashchekina Y, Chabina A, Konson V, Nashchekin A, Mikhailova N. Carboxymethyl cellulose in composite collagen gel improves mesenchymal stromal cell proliferation and migration. Int J Biol Macromol. 2025;319(1):145418. doi:10.1016/j.ijbiomac.2025.145418.
20. Ji Q, Zhang Z, Han Y, Zhang Y, Zhou A, Xu J, et al. Novel bacterial cellulose composite material prepared by the synergistic deposition of collagen and Tannin. ACS Sustain Chem Eng. 2025;13(41):17208–19. doi:10.1021/acssuschemeng.5c05306.
21. Tang P, Lu Y, Li X, Zheng T. Novel multifunctional collagen-based food packaging film incorporating with bilberry anthocyanin for freshness monitoring. Food Packag Self Life. 2025;49(2):101508. doi:10.1016/j.fpsl.2025.101508.
22. Wang W, Wang Y, Wang Y, Zhang X, Wang X, Gao G. Fabrication and characterization of microfibrillated cellulose and collagen composite films. J Bioresour Bioprod. 2016;1(4):162–8. doi:10.21967/JBB.V1I4.54.
23. Farooq S, Ahmad ML, Zheng S, Ali U, Li Y, Cui S, et al. A review on marine collagen: sources, extraction methods, colloids properties, and food applications. Collagen Leather. 2024;6(1):11. doi:10.1186/s42825-024-00152-y.
24. Yin S, Zhang Y, Zhang X, Tao K, Li G. High-strength collagen/delphinidin film incorporated with Vaccinium oxycoccus pigment for active and intelligent food packaging. Collagen Leather. 2023;5(1):11. doi:10.1186/s42825-023-00118-6.
25. Panahirad S, Dadpour M, Peighambardoust SH, Soltanzadeh M, Gullon B, Alirezalu K, et al. Applications of carboxymethyl cellulose- and pectin-based active edible coatings in preservation of fruits and vegetables: a review. Trends Food Sci Technol. 2021;11(4):663–73. doi:10.1016/j.tifs.2021.02.025.
26. Padhan B, Patel R, Bhowmik P, Roy A, Das J, Yu Y, et al. Recent advancements in nanocomposites-based antibiofilm food packaging. J Polym Mater. 2025;42(2):411–43. doi:10.32604/jpm.2024.059156.
27. Ghosh S, Mandal RK, Mukherjee A, Roy S. Nanotechnology in the manufacturing of sustainable food packaging: a review. Discov Nano. 2025;20(1):36. doi:10.1186/s11671-025-04213-x.
28. Ashfaq A, Khursheed N, Fatima S, Anjum Z, Younis K. Application of nanotechnology in food packaging: pros and Cons. J Agric Food Res. 2022;7(9):100270. doi:10.1016/j.jafr.2022.100270.
29. Herrera-Rivera MR, Torres-Arellanes SP, Cortes-Martinez CI, Navarro-Ibarra DC, Hernandez-Sanchez L, Solis-Pomar F, et al. Nanotechnology in food packaging materials: role and application of nanoparticles. RSC Adv. 2024;14(30):21832–58. doi:10.1039/d4ra03711a.
30. Assanvo EF, N'Gatta KM, Toure KJ-VN, Konan AM, Boa D. Extraction and detailed physico-chemical characterization of lignocellulosic fibers derived from *Lonchocarpus cyanescens*. J Polym Mater. 2024;41(2):55–68. doi:10.32604/jpm.2024.055397.
31. Abolore RS, Jaiswal S, Jaiswal AK. Green and sustainable pretreatment methods for cellulose extraction from lignocellulosic biomass and its applications: a review. Carbohydr Polym Technol Appl. 2024;7(29):100396. doi:10.1016/j.carpta.2023.100396.
32. Kakati N, Assanvo EF, Kalita D. Alkalinization and graft copolymerization of pineapple leaf fiber cellulose and evaluation of physic-chemical properties. Polym Compos. 2019;40(4):1395–403. doi:10.1002/pc.24873.

33. Cai J, He Y, Yu X, Banks SW, Yang Y, Zhang X, et al. Review of physicochemical properties and analytical characterization of lignocellulosic biomass. Renew Sustain Energy Rev. 2017;76:309–22. doi:10.1016/j.rser.2017.03.072.
34. Nagaraja S, Easwaramoorthi S, Rao JR, Thanikaivelan P. Probing visible light induced photochemical stabilization of collagen in green solvent medium. Int J Biol Macromol. 2019;131(5):779–86. doi:10.1016/j.ijbiomac.2019.03.109.
35. Momeni S, Ghomi ER, Shakiba M, Shafiei-Navid S, Abdouss M, Bigham A, et al. The effect of poly (Ethylene glycol) emulation on the degradation of PLA/starch composites. Polymers. 2021;13(7):1019. doi:10.3390/polym13071019.
36. Biesta-Peters EG, Reij MW, Joosten H, Gorris LGM, Zwietering MH. Comparison of two optical-density-based methods and a plate count method for estimation of growth parameters of bacillus cereus. Appl Environ Microbial. 2010;76(5):1399–1405. doi:10.1128/AEM.02336-09.
37. Ferreira JM, Capela C, Manaia J, Costa JD. Mechanical properties of woven mat Jute/epoxy composites. Mater Res. 2016;19(3):702–10. doi:10.1590/1980-5373-MR-2015-0422.
38. Barefoot SF, Klaenhammer TR. Detection and activity of lactacin B, a bacteriocin produced by lactobacillus acidophilust. Appl Environ Microbiol. 1983;45(6):1808–15. doi:10.1128/aem.45.6.1808-1815.1983.
39. Hwanhlem N, Buradaleng S, Wattanachant S, Benjakul S. Isolation and screening of lactic acid bacteria from Thai traditional fermented fish (Plasom) and production of Plasom from selected strains. Food Control. 2011;22(3–4):401–7. doi:10.1016/j.foodcont.2010.09.010.
40. Secario MK, Truong TTV, Chen C-C, Lai J-Y, Lue SJ. Size-dependent antibacterial efficacy of silver nanoparticles from a green synthesis method: effects of extract quantity and origin. J Taiwan Inst Chem Eng. 2024;161:105511. doi:10.1016/j.jtice.2024.10551.
41. Menichetti A, Mavridi-Printezi A, Mordini D, Montalti M. Effect of size, shape and surface functionalization on the antibacterial activity of silver nanoparticles. J Funct Biomater. 2023;14(5):244. doi:10.3390/jfb14050244.
42. Da Silva BL, Caetano BL, Chiari-Andréoa BG, Pietro RCLR, Chiavacci LA. Increased antibacterial activity of ZnO nanoparticles: influence of size and surface modification. Colloids Surf B Biointerfaces. 2019;177:440–7. doi:10.1016/j.colsurfb.2019.02.013.
43. Sirivallop A, Areerob T, Chiarakorn S. Enhanced visible light photocatalytic activity of N and Ag doped and co-doped TiO_2 synthesized by using an *In-Situ* solvothermal method for gas phase ammonia removal. Catalysts. 2020;10(2):251. doi:10.3390/catal10020251.
44. Liu C, Geng L, Yu Y, Zhang Y, Zhao B, Zhao Q. Mechanisms of the enhanced antibacterial effect of Ag-TiO_2 coatings. Biofouling. 2018;34(2):190–9. doi:10.1080/08927014.2017.1423287.
45. Ali T, Ahmed A, Alam U, Uddin I, Tripathi P, Muneer M. Enhanced photocatalytic and antibacterial activities of Ag-doped TiO_2 nanoparticles under visible light. Mater Chem Phys. 2028;212(9):325–35. doi:10.1016/j.matchemphys.2018.03.052.
46. Marouazi HE, Abdouli I, Essayem N, Guillard C, Keller V, Janowska I. Efficient and selective glucose conversion in a low temperature photocatalysis-assisted hydrothermal process over TiO_2-few layer graphene and Ta-doped TiO_2 (photo) catalysts. Cleaner Chem Eng. 2025;11:100205. doi:10.1016/j.clce.2025.100205.
47. Rao MMV, Mohammad N, Banerjee S, Khanna PK. Synthesis and food packaging application of silver nanoparticles: a review. Hybrid Adv. 2024;6(4):100230. doi:10.1016/j.hybadv.2024.100230.
48. Akhavan O. Lasting antibacterial activities of Ag-TiO_2/Ag/a-TiO_2 nanocomposite thin film photocatalysts under solar light irradiation. J Colloid Interface Sci. 2009;336(1):117–24. doi:10.1016/j.jcis.2009.03.018.
49. Liza TZ, Tusher MMH, Anwar F, Monika MF, Amin KF, Asrafuzzaman FNU. Effect of Ag-doping on morphology, structure, band gap and photocatalytic activity of bio-mediated TiO_2 nanoparticles. Results Mater. 2024;22(4):100559. doi:10.1016/j.rinma.2024.100559.
50. Nguyen MT, Ha PT, Le TTH, Bui HG, Phan KS, Chu NH, et al. A floatable TiO_2–Ag photocatalyst enables effective antibiotic degradation and pathogen growth control. RSC Adv. 2025;15(23):18324–37. doi:10.1039/D5RA02333E.
51. Sati A, Ranade TN, Mali SN, Yasin HKA, Pratap A. Silver nanoparticles (AgNPs): comprehensive insights into bio/synthesis, key influencing factors, multifaceted applications, and toxicity—a 2024 update. ACS Omega. 2025;10(8):7549–82. doi:10.1021/acsomega.4c11045.

52. Joshi G, Naithani S, Varshney VK, Bisht SS, Rana V, Gupta PK. Synthesis and characterization of carboxymethyl cellulose from office waste paper: a greener approach towards waste management. Waste Manag. 2025;38:33–40. doi:10.1016/j.wasman.2014.11.015.
53. Assanvo EF, Nagaraj S, Boa D, Thanikaivelan P. Hybrid collagen-cellulose–Fe_3O_4@TiO_2 magnetic bio-sponges derived from animal skin waste and Kenaf fibers for wastewater remediation. Sci Rep. 2023;13(1):13365. doi:10.1038/s41598-023-40520-y.
54. Aigaje E, Riofrio A. Processing, properties, modifications, and environmental impact of nanocellulose/biopolymer composites: a review. Polymers. 2023;15:1219. doi:10.3390/polym1505121.
55. Anaya-Esparza LM, Ruvalcaba-Gomez JM, Maytorena-verdugo CI, Gonzalez-Silva N, Romero-toledo R, Aguilera-Aguirre S, et al. Chitosan-TiO_2: a versatile hybrid composite. Materials. 2020;13(4):811. doi:10.3390/ma13040811.
56. Ma X, Zare Y, Rhee KY. A two-step methodology to study the influence of aggregation/agglomeration of nanoparticles on young's modulus of polymer nanocomposites. Nanoscale Res Lett. 2017;12(1):621. doi:10.1186/s11671-017-2386-0.
57. Ghanbarzadeh B, Almasi H. Physical properties of edible emulsified films based on carboxymethyl cellulose and oleic acid. Int J Biol Macromol. 2011;48(1):44–9. doi:10.1016/j.ijbiomac.2010.09.014.
58. Priyadarshi R, Kim S-M, Rhim J-W. Carboxymethyl cellulose-based multifunctional film combined with zinc oxide nanoparticles and grape seed extract for the preservation of high-fat meat products. Sustain Mater Technol. 2021;29:e00325. doi:10.1016/j.susmat.2021.e00325.
59. Xing L, Hu C, Zhang W, Guan L, Gu J. Transition of cellulose supramolecular structure during concentrated acid treatment and its implication for cellulose nanocrystal yield. Carbohydr Polym. 2020;229(1):115539. doi:10.1016/j.carbpol.2019.115539.
60. Yue C, Ding C, Yang N, Luo Y, Su J, Gao L, et al. Strong and tough collagen/cellulose nanofibril composite films via the synergistic effect of hydrogen and metal-ligand bonds. Eur Polym J. 2022;180(18):111628. doi:10.1016/j.eurpolymj.2022.111628.
61. Muke D, Bilasi M, Jérémie LM, Pierre O, Lohohola1, Omer MM, et al. Évaluation de l'effet bactericide des nanostructures sol-gel de TiO_2 intrinseque et Ag-TiO_2 dope sur Escherichia coli, Pseudomonas aeruginosa et Staphylococcus aureus. J Afri Sci. 2024;1(2):157–69. doi:10.70237/jafrisci 2024.v1.i2.16.